Open access • Journal Article • DOI:10.1063/1.3081884

Structural analysis of ultrafast extended x-ray absorption fine structure with subpicometer spatial resolution: application to spin crossover complexes.

Wojciech Gawelda, Van-Thai Pham, R. M. van der Veen, Daniel Grolimund ...+4 more authors

Institutions: École Polytechnique Fédérale de Lausanne, Paul Scherrer Institute

Published on: 31 Mar 2009 - Journal of Chemical Physics (American Institute of Physics)

Topics: Surface-extended X-ray absorption fine structure, Ground state, Extended X-ray absorption fine structure, Excited state and Absorption spectroscopy

The Journal of Chemical Physics

Structural analysis of ultrafast extended x-ray absorption fine structure with subpicometer spatial resolution: Application to spin crossover complexes

W. Gawelda, V.-T. Pham, R. M. van der Veen, D. Grolimund, R. Abela et al.

Citation: J. Chem. Phys. **130**, 124520 (2009); doi: 10.1063/1.3081884
View online: http://dx.doi.org/10.1063/1.3081884
View Table of Contents: http://jcp.aip.org/resource/1/JCPSA6/v130/i12
Published by the American Institute of Physics.

THE JOURNAL OF CHEMICAL PHYSICS **130**, 124520 (2009)

Structural analysis of ultrafast extended x-ray absorption fine structure with subpicometer spatial resolution: Application to spin crossover complexes

W. Gawelda,[1,2,a)] V.-T. Pham,[1] R. M. van der Veen,[1] D. Grolimund,[2] R. Abela,[2]
M. Chergui,[1,b)] and C. Bressler[1,2]
[1] *Ecole Polytechnique Fédérale de Lausanne, Laboratoire de Spectroscopie Ultrarapide, Institut des Sciences et Ingénierie Chimiques, CH-1015 Lausanne-Dorigny, Switzerland*
[2] *Swiss Light Source, Paul Scherrer Institut, CH-5232 Villigen PSI, Switzerland*

(Received 31 October 2008; accepted 26 January 2009; published online 31 March 2009)

We present a novel analysis of time-resolved extended x-ray absorption fine structure (EXAFS) spectra based on the fitting of the experimental transients obtained from optical pump/x-ray probe experiments. We apply it to the analysis of picosecond EXAFS data on aqueous $[\mathrm{Fe^{II}(bpy)_3}]^{2+}$, which undergoes a light induced conversion from its low-spin (LS) ground state to the short-lived ($\tau \approx 650$ ps) excited high-spin (HS) state. A series of EXAFS spectra were simulated for a collection of possible HS structures from which the ground state fit spectrum was subtracted to generate transient difference absorption (TA) spectra. These are then compared with the experimental TA spectrum using a least-squares statistical analysis to derive the structural change. This approach reduces the number of required parameters by cancellation in the differences. It also delivers a unique solution for both the fractional population and the extracted excited state structure. We thus obtain a value of the Fe–N bond elongation in the HS state with subpicometer precision (0.203 ± 0.008 Å). © *2009 American Institute of Physics*. [DOI: 10.1063/1.3081884]

I. INTRODUCTION

Structural dynamics is a rapidly developing field which aims at monitoring the geometric structural changes in the course of a chemical reaction, a biological function, or a phase transition.[1–4] Over the last few years, time-resolved x-ray absorption spectroscopy (XAS), exploiting pulsed laser and synchrotron radiation in a pump-probe configuration, has been established as a new tool to explore both the electronic and geometric structure changes of short-lived excited states via analysis of its x-ray absorption near edge structure (XANES) or extended x-ray absorption fine structure (EXAFS).[1,2,4,5] Experiments with hard x rays ($E > 2$ keV) were performed with a temporal resolution of 50–100 ps, limited by the pulse width of electron bunches currently available at third generation storage rings. A recent add on to synchrotrons (the so-called femtosecond slicing scheme) has been implemented to deliver tunable x-radiation of femtosecond duration,[6] and the probing of ultrafast dynamics of a molecular system in liquids has been achieved for the first time using XAS with a resolution of 250 fs.[7]

In view of these developments, which offer the possibility to probe molecular motion in real time by taking snapshots of structural changes step by step, it is becoming important to establish methods that retrieve precise quantitative structural information about the light-induced changes in x-ray absorption spectra. While the current studies deal with equilibrium structures of reaction intermediates that represent relaxation bottlenecks on the picosecond time scale, this is already changing with the femtosecond XAS transient of the molecular system mentioned above.[7] We therefore approach the time resolution needed to tackle the evolving structures of molecular transition states, which are central to chemical reactivity and dynamics.[8]

Our approach to optical pump/x-ray absorption probe experiments[1,4,9] has been based on the transient difference absorption (TA) method, where the x-ray transmission through the sample is recorded at twice the repetition rate of the pump laser (typically, 1 kHz), such that the laser-pumped and the unexcited sample transmission are recorded and their absorption difference taken on a shot-to-shot basis.[1,9,10] This method has the advantage of correcting for effects of long term drifts of the source intensity and/or the deterioration of samples under synchrotron and laser irradiation. It especially eliminates the uncertainty in energy between the pumped and unpumped XAS spectra, as the several thousand laser-on/laser-off XAS intensities are measured in rapid alternation for every energy point of the primary monochromator.[9] Finally, we achieve a high sensitivity using this scheme, thanks also to the high stability of synchrotron sources. With this approach, we detected (down to 50 ps time delay) the electronic and geometric structure changes of a ruthenium-based molecular complex upon light-induced intramolecular electron transfer,[11,12] the structural changes due to the light-induced spin crossover (SCO) process in an Fe(II) molecular complex,[13] and the solute and solvent changes in photoexcited aqueous iodide.[4,14] Here we concentrate on the SCO complexes.

In our previous work,[13] the structure of aqueous

[a)] Present address: Laser Processing Group, Instituto de Óptica, CSIC, Serrano 121, E-28006 Madrid, Spain.

[b)] Electronic mail: majed.chergui@epfl.ch.

$[\mathrm{Fe^{II}(bpy)_3}]^{2+}$ in the high spin (HS) lowest excited state was determined by two methods: (a) in the first, we directly fitted the XANES region of the transient (difference) spectrum in energy space using the MXAN code; (b) in the second, we extracted the XAS spectrum of the HS state using the difference and ground state (GS) XAS spectra and carried out a standard EXAFS analysis on it. Both approaches rely on the prior knowledge of the photoexcitation yield, which was determined in a separate laser-only experiment. The results of both approaches yielded an elongation of the Fe–N bond by about 0.2 Å from the low spin (LS) GS to the HS state.

Because the recorded data are a transient *difference* spectrum, here we present an analysis based on the direct fitting of the EXAFS region of the transient spectrum. The TA spectrum contains *all* the information on laser-induced spectral changes at a given time delay with the advantage of avoiding systematic errors during the independent fitting of ground and excited state spectra. The power of fitting transient EXAFS spectra was already demonstrated by Pettifer *et al.*[15] who reported a precision on the femtometer length scale of a magnetostrictive system. In their approach, they used a first-order Taylor expansion of the EXAFS equation to fit the differential EXAFS at the Fe *K*-edge of an Fe–Co thin film. This approach works fine for minute structural changes on the femtometer length scale (about 10^{-4} Å) but cannot be generalized toward much larger local structural changes, as presented here.

In chemical systems, light-induced bond changes are on the order of tenths of an angstrom, and the ionization threshold may also change as a result, with the consequence that the photoelectron wave vector can no longer be referenced to the ionization energy of the GS molecule. Such shifts are on the order of 1–2 eV, and although the EXAFS region spans up to several hundreds of eV, caution is nevertheless needed if the structural changes are small, or if they have to be determined with high precision. Therefore, a more general treatment of transient EXAFS should take into consideration possible changes in the ionization energy. In the procedure adopted here, we use the GS structural parameters and simulate the EXAFS spectra for a series of different possible (but chemically reasonable) excited state structures by a stepwise variation in the Fe-ligand bond distance while keeping the ligand structure unchanged. We compare the calculated transient EXAFS spectra with the transient experimental data in a statistical analysis. Hereby we depart from conventional practice and analyze the nonweighted EXAFS (with respect to the photoelectron wave vector k). Last, this is all performed in energy space. The statistical analysis is possible since we use the experimental uncertainty for each individual data point as a quantitative measure of the agreement between spectrum and simulation, and therefore we no longer need to worry about biasing the EXAFS content at any value of k. This treatment should serve as a stepping stone toward a refined analysis of femtosecond EXAFS spectra of chemical species that are starting to be obtained.[7]

The present study deals with a molecular reaction cycle, which can be described as a two-state system within the experimental time resolution. However, the analysis can be extended to include more states as well. The presence of merely a LS and HS species in our experiment[13] is supported by the laser-only studies we carried out as a function of pump laser intensity on all time scales within the lifetime of the entire reaction cycle.[16] Only for pump intensities exceeding those of the time-resolved XAS measurements (typically 0.2–0.25 mJ on a 0.35 mm spot) by a factor of 2 did we detect a contribution of multiphoton absorption processes of around 4%, and therefore we can safely assume that we are dealing with a two-state system only. Next, the large x-ray pulse width of 100 ps (full width at half maximum) will in principle sample populations from time zero up to about 70 ps, and thus the signal may consist of a mixture of various different structures. However, the LS→HS conversion itself is complete within 300 fs,[7] which would negligibly contribute to the averaged structure analysis (to less than 0.5%). Finally, we recently measured vibrational cooling in HS state and found that it occurs in <4 ps,[17] and this can affect the averaged Debye-Waller (DW) factor for the HS species (when convoluting with the x-ray pulse width), but to less than about 5%. Such minute changes do not significantly affect the calculated EXAFS spectrum. In short, we can safely assume that we are dealing here with a two-level system.

II. TIME-RESOLVED EXTENDED X-RAY ABSORPTION FINE STRUCTURE SPECTROSCOPY

The (static) EXAFS is a measure of the local environment around an absorbing atom. It is described as a function of the photoelectron wave vector k via the so-called EXAFS equation

$$\chi(k) = \sum_j \frac{S_0^2 N_j f_j(k)}{kR_j^2} \cdot e^{-2R_j/\lambda(k)} \cdot e^{-2k^2\sigma_j^2} \cdot \sin[2kR_j + \delta_j(k)] \tag{1}$$

with the index j classifying shells of identical backscatterers, each accompanied by their coordination number N_j, backscattering amplitude f_j, distance R_j with a mean square fluctuation of σ_j^2 (DW factor), and δ_j describing the k-dependent central atom phase shift in the absorber, which decreases linearly with k for all elements. Finally, S_0^2 and $\lambda(k)$ are the amplitude reduction factor and the mean free path of the photoelectron wave, respectively.

As already mentioned, in our picosecond EXAFS experiment we measure a reaction intermediate that represents a bottleneck of the relaxation pathway of the system. We demonstrated[4] that its structure can be obtained from the TA spectrum $\Delta A(E,t)$ at a given time delay t, which is related to the excited state spectrum $A_{\mathrm{ES}}(E,t)$ at time t via the relationship

$$\Delta A(E,t) = f(t)[A_{\mathrm{ES}}(E,t) - A_{\mathrm{GS}}(E)] \tag{2}$$

with $A_{\mathrm{GS}}(E)$ being the reactant (or static) spectrum and f being the fractional population in the excited state. Whenever a certain process generates n different reaction products with associated spectra A_n we have to consider

$$\Delta A(E,t) = \sum_n f_n(t)[A_n(E,t) - A_{\mathrm{GS}}(E)] \tag{3}$$

respecting

$$\sum_n f_n(t) = f_{\mathrm{exc}}(t) \tag{4}$$

at all times and $f_{\mathrm{exc}}(t)$ being the total fraction of molecules removed from the GS population. When dealing with reaction intermediates, the excited state x-ray absorption spectrum $A_{\mathrm{ES}}(E)$ *does not* depend on time t but only on its population $f(t)$. Thus the time dependence for A_{ES} in Eqs. (2) and (3) can be removed. However, on the ultrafast (femtosecond) time scale it will become possible to measure the EXAFS of transition states,[7] and for this case we do expect a time-dependent change in the excited state spectrum $A_{\mathrm{ES}}(E,t)$, thus Eqs. (2) and (3) include the extension toward femtosecond time resolution. In the present analysis the only time-dependent parameter, which strongly modulates $\Delta A(t)$, is the fractional population $f(t)$, which is directly derived during the analysis.

In a standard EXAFS analysis, a measured spectrum, e.g., $A_{\mathrm{GS}}(E)$, is normalized with a function $g(E)$, such that the absorption edge jump is unity at all energies above the edge,[1] e.g., by normalizing it with the gas-phase spectrum consisting of the single central atom. Subsequently, one isolates the EXAFS modulations/oscillations in energy space $\chi_{\mathrm{GS}}(E)$ by subtracting unity from the normalized spectrum $A_{\mathrm{GS}}(E)$. Applying the same normalization as for $A_{\mathrm{GS}}(E)$ to the measured transient absorption spectrum in Eq. (2) will thus generate the *transient* EXAFS function $\Delta\chi(E,t)$,

$$\begin{aligned}\Delta A(E,t)g(E) &= f(t)[A_{\mathrm{ES}}(E) - A_{\mathrm{GS}}(E)]g(E)\\ &= f(t)[\chi_{\mathrm{ES}}(E) - \chi_{\mathrm{GS}}(E)] = f(t)\Delta\chi(E),\end{aligned} \tag{5}$$

although now without any time dependence of the transient EXAFS function for the case of a mere two-level system. This normalization is valid since the atomic background remains identical for both the ground and excited state EXAFS around the same central atom. Likewise, Eq. (5) can be extended to the case of Eq. (3) including several different excited states, since the reactant GS normalization $g(E)$ can nevertheless be applied in the normalization procedure for each excited state species n.

The conventional fitting routine in EXAFS follows Eq. (1) after translating the x-ray energy of the EXAFS into the photoelectron wave vector via $k=((E-E_0)2m_e/\hbar^2)^{1/2}$ and applying k^n weighting to the result

$$\Delta\chi(E,t) \Rightarrow \Delta\chi(k,t)k^m, \tag{6}$$

where one can alter the parameters of each coordination shell j individually. The k^m weighting is applied to emphasize changes in the EXAFS at low k (for small m values) or at high k values (for larger m). However, while this additional weighting certainly serves display purposes, it remains unnecessary for the present statistical analysis, which includes the experimental error for each data point, and thus avoids biasing any features observed throughout the entire EXAFS region.

For the analysis, one starts with an *a priori* knowledge of the investigated sample, often including a rather precise knowledge of the distance to the shell of nearest neighbors. The fit procedure then optimizes this distance to generate the closest match to the measured EXAFS. However, when the shell distance needs to be significantly modified, the result might violate the chemical properties of the sample. For $[\mathrm{Fe^{II}(bpy)_3}]^{2+}$, an example would be to simply move an entire coordination shell [here, the nearest neighboring N atoms, Fig. 1(a)] without respecting the integrity of the bpy ligand structure, which is known to be rigid. We take this into account by moving the entire bpy ligand by a certain distance without modifying its internal structure [Fig. 1(b)], and the resulting EXAFS calculation with Eq. (1) should thus become chemically meaningful.

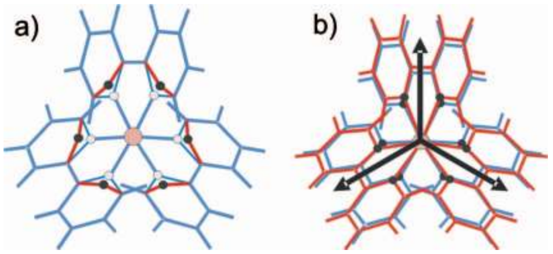

FIG. 1. (Color) (a) Sketch of the effect of shell fitting by moving an entire coordination shell. Here, the Fe–N distance in $[\mathrm{Fe^{II}(bpy)_3}]^{2+}$. Such a treatment distorts the structure of the bpy ligands. (b) This can be avoided by locking the bpy structure and moving each ligand by a certain distance along their trigonal axis implying a consequent change in the N–Fe–N angle.

In this paper, our analysis of the HS state of photoexcited aqueous $[\mathrm{Fe^{II}(bpy)_3}]^{2+}$ data is based on iterative simulations of EXAFS spectra using the FEFF code[18] to calculate several different structural models of the excited state structure. We have not limited ourselves to a single shell treatment but use the entire molecular cluster to calculate the HS EXAFS with a stepwise and gradual elongation of Fe-bpy bonds according to Fig. 1(b) using the CERIUS2 molecular visualization environment program.[19] We start off with the LS GS structure from crystallographic data[20] for which we optimized the parameters in Eq. (1) by fitting our experimental GS spectrum. This treatment delivers reliable values of the nonstructural parameters including the thermal disorder (DW factors). With these GS parameters locked, we simulate a series of EXAFS spectra for various distance changes between Fe and the bpy ligands in steps of up to 0.03 Å (relative to the GS Fe–N bond length of 1.98 Å) from 0 to 0.45 Å [as shown for two examples in Fig. 1(b)]. With these HS EXAFS spectra we calculate the difference spectra which we compare to the experimental TA data in a rigorous statistical analysis. The detailed steps of this treatment are given below.

III. DATA TREATMENT AND STRUCTURAL SIMULATIONS

As already mentioned, the experiment implies the simultaneous measurement of the GS (static) EXAFS and the TA spectrum, as described in Refs. 9, 10, and 21. The resulting spectra are shown in Fig. 2 after both have received the same postedge normalization. The GS EXAFS is then fitted (Fig. 3) to refine the structural parameters including all DW factors σ_j. For example, for the latter we obtain $\sigma_j^2=6(1)$

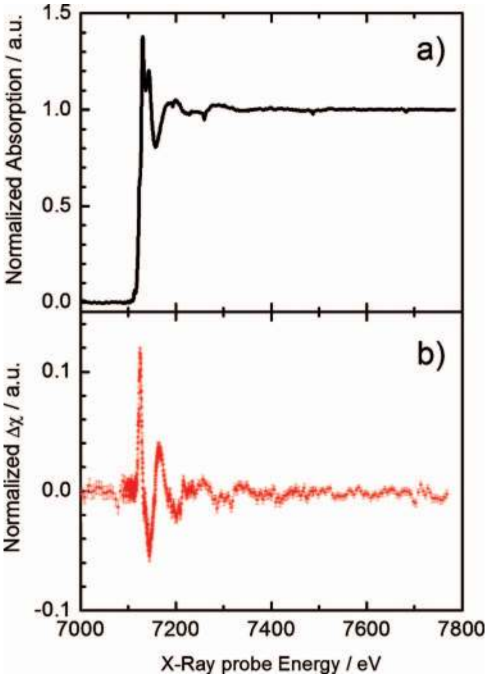

FIG. 2. (Color) (a) XAS of aqueous $[\mathrm{Fe^{II}(bpy)_3}]^{2+}$ and (b) transient XAS at 50 ps time delay after laser excitation.

$\times 10^{-3}$ Å^2 in agreement with the values previously determined for similar compounds.[22,23] This fit curve is then the EXAFS spectrum of the reactant structure (or reactant model m_0, hereafter, m denotes the EXAFS spectra)

$$m_0(k) = \chi_0(k). \tag{7}$$

Next, we calculate the EXAFS for several different structures by moving the bpy ligands radially by a certain amount ΔR_i away from the central Fe atom, each one along its associated trigonal symmetry axis [see Fig. 1(b)], as illustrated in Figs. 4(a) and 4(b). The parameters in Eq. (1) are kept constant including the intraligand angles (except the distances R_i, of course) when calculating the EXAFS of the different excited state models m_i. We simulated the EXAFS spectra for ΔR_i increments of 0.03 Å between 0.03 and 0.45 Å, corresponding to $i=1-15$ [with $R_0(\mathrm{Fe-N})=1.98$ Å (Ref. 20)]. In addition, in the range between 0.15 and 0.21 Å, we interpolated the spectra m_i and m_{i+1} in finer steps of 0.005 Å. This (linear) interpolation is justified as we cross checked the 0.18 Å spectrum ($=m_6$) with the interpolated result using the 0.15 and 0.21 Å simulations (thus, $m_6'=0.5(m_5+m_7)$) without observing a significant deviation between m_6' and m_6.

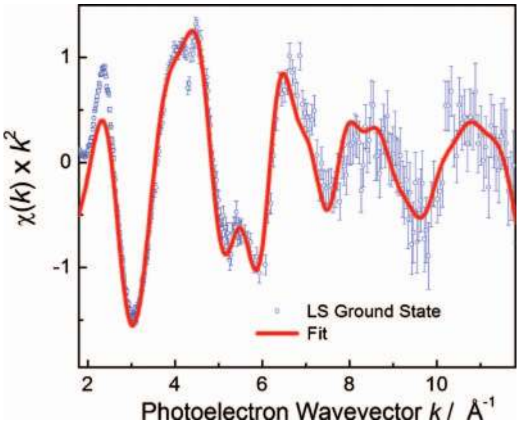

FIG. 3. (Color) GS EXAFS of $[\mathrm{Fe^{II}(bpy)_3}]^{2+}$ together with its fit to Eq. (1) delivering the reactant EXAFS spectrum $m_0(k)$, whose parameters are kept constant for the calculation of the excited state EXAFS spectra $m_i(k)$ for several structures with the Fe–N distance set to R_i by moving each bpy ligand symmetrically by ΔR_i along their associated trigonal axis.

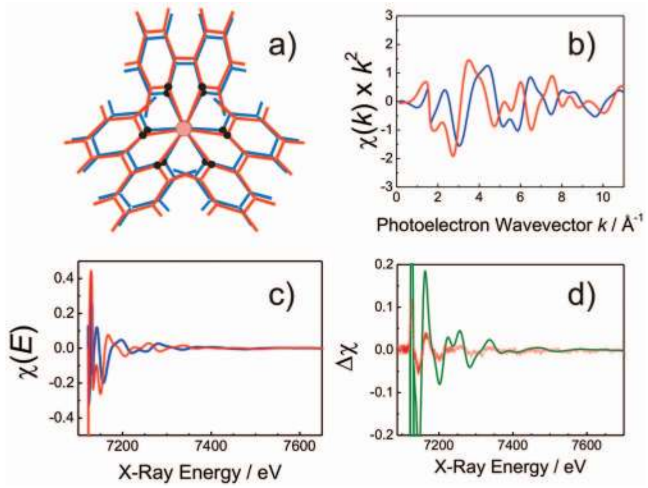

FIG. 4. (Color) Sketch of the procedure to generate transient EXAFS spectra shown for two structures: (a) geometrical representation of the input structures used for calculating the EXAFS; (b) k^2-weighed EXAFS spectra calculated from (a) as a function of the photoelectron wave vector k; (c) back-transformed EXAFS spectra to energy space (and removing the k^2 weighing) so that the GS EXAFS coincides with the GS calculation; (d) for two different structures, the transient spectrum is calculated and shown for comparison with the actual transient data (not yet scaled according to the fractional population).

Now we can simulate the TA spectrum (labeled tr_i) for each distance model with R_i by calculating the difference spectrum between each excited state spectrum m_i and the reactant spectrum via

$$tr_i(k) = m_i(k') - m_0(k). \tag{8}$$

In Fig. 4(b), this would be the difference between the two curves (after removing the k^2 weighting). However, as already mentioned above, excited molecules may have a different ionization threshold than in the GS species. The extreme case would be that of reduction or oxidation processes, see, e.g., Ref. 12, but also the altered electronic structure of the excited state may affect the ionization threshold, and as a consequence, the position of $k=0$ for the excited state EXAFS. This is the reason for the notation k' in Eq. (8). This seriously complicates the calculation of the transient spectrum since (i) $k=0$ is different for m_i and m_0, and thus (ii) the k^2 weighting would be no longer correct for the XAS spectrum of the excited state when keeping the same ionization threshold as in the GS. The excited state EXAFS (for the HS species) may experience an energy shift

$$\Delta E_0 = E_0^{\mathrm{HS}} - E_0^{\mathrm{LS}} \tag{9}$$

with respect to the LS EXAFS with E_0 being the ionization potential for the superscripted species. To account for this shift we have removed the k^2 weighting of the calculated spectra m_i in Fig. 4(b) and back transformed the EXAFS spectra into energy space, as shown in Fig. 4(c). Hereby, we made sure that the LS EXAFS function $m_0(E)$ accurately matches the experimental LS EXAFS in energy space. We can then shift the excited state models m_i horizontally with respect to m_0 (which is not and may never be shifted) by ΔE_0,

$$m_i(E) \rightarrow m_i(E + \Delta E_0). \tag{10}$$

With these spectra we finally calculate the transient EXAFS by subtracting each new distance model (its spectrum) from that of the GS via

$$tr_i(E) = m_i(E + \Delta E_0) - m_0(E). \tag{11}$$

One result is illustrated in Fig. 4(d). For the comparison simulation experiment, according to Eq. (5), they should then be scaled by the fractional excited state population f; in other words, Eq. (11) uses $f=1$.

IV. STATISTICAL ANALYSIS OF THE EXPERIMENT

In order to determine the HS structure accurately we calculate the residuals between each transient model and the transient data and evaluate their goodness by the reduced chi squared function χ_r^2 [not to be confused with the EXAFS function χ, Eq. (1)] via

$$\chi_r^2(i,f,\Delta E_0) = \frac{1}{(N-1)} \sum_{j=1}^{N} \left(\frac{x_j/f - tr_j^i(\Delta R_i, \Delta E_0)}{\Delta x_j/f} \right)^2 \tag{12}$$

within a selected range of N data points, x_j being the experimental data point j from the transient measurement [with experimental error Δx_j, and both scaled with $1/f$ according to Eq. (5)] and tr_j^i (i denotes the spectrum derived from the structural model with an R_i distance between the Fe and N atoms) being the simulated transient value for a given new Fe-bpy distance change ΔR_i calculated after including the (chemical) energy shift ΔE_0 for the excited state spectra.

We calculated a large series of residuals for selected values of ΔE_0 (-2.5, -1.8, -1.2, -0.6, and 0 eV) by changing the value of f from 12% to 28% in steps of 1% and computing their χ_r^2 values, as shown in Fig. 5. The plots show multiple curves, each connecting the χ_r^2 values for a given f value [e.g., the thick lines in Figs. 5(a)–5(c) connect the results for f=22%]. The χ_r^2 values were calculated using 296 data points from the experimental spectrum in energy space; translating these energies into wave vector space shows that they cover the 1.8–10.1 Å^{-1} range (of the LS molecule). In an identical treatment to that shown in Fig. 5, we also carried out the residual analysis for the 2–8.5 Å^{-1} range (245 points) as well as to all possible data points (394). One observes for each series nearly the same global minimum, which corresponds to the Fe–N bond distance increment, as shown in Fig. 5.

The ΔR at minimum depends on the choice of chemical shift ΔE_0, as illustrated in Fig. 6 for both data ranges. The least-squares analysis yields a global minimum for ΔE_0=-1.2 eV in both cases, -0.6 eV may appear acceptable as well, but -1.8 eV is not acceptable for the extended data range. Therefore, from the figure we may consider values between approximately -0.5 and -1.5 eV as the acceptable range for ΔE_0. The error bars in Fig. 6(b) were determined by the (arbitrary) condition that all χ_r^2 values (and thus Fe–N distances R_i) are acceptable, which do not increase the least-squares value by more than 10% (=90% confidence level). This is certainly justified by the fact that adjacent χ_r^2 values around the minima in Fig. 5 change by typically 2% or less, and adjacent points follow a general (not arbitrary) pattern. This would also justify restricting this condition to less than 5% (=95% confidence level), which we consider closer to the actual accuracy limit of this simulation series, and thus the 90% confidence level remains rather conservative. The possible bond length change is also influenced by the (assumed) fractional HS population f, as clearly seen in Fig. 5. This can also be influenced by fluctuating laser energies during the measurement, and a precise value of this quantity including its standard deviation is necessary to obtain a precise excited state structure when no other means are available than the laser-only input. We have consequently analyzed the influence of f on the square residuals. Figure 7 shows the least-squares analysis assuming a constant fractional population of 15%, 17%, 19%, and 22%. For f values above 20% the χ_r^2 values minimize towards positive chemical shift values. The previous analysis suggests that we accept only f-values with a least-squares (minimum) around -1.2 eV, thus making the curves for 17% acceptable, while both 15% and 19% move the minimum outside the accepted range for ΔE_0, as derived above. Thus we obtain a fractional population of 17(1)%. Therefore, this analysis solved Eq. (2), which contains two unknowns, fractional population and the

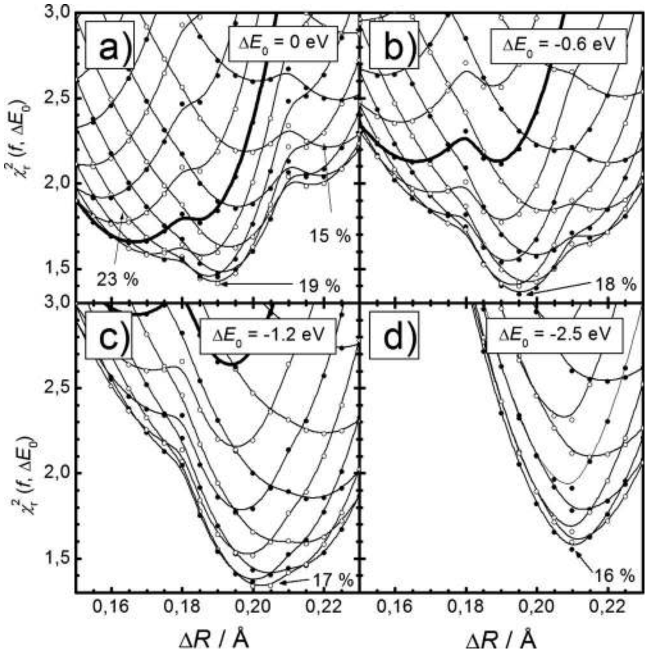

FIG. 5. Square residuals between the experimental data and transient simulations [Eq. (11)] for the $[\mathrm{Fe^{II}(bpy)_3}]^{2+}$ excited state structure by moving the entire bpy ligands in steps of 0.005 Å in the ΔR range from 0.15–0.23 Å. The curves serve as a guide to the eyes and connect the χ_r^2 values for a fixed f-value (varied in steps of 1% from 12%–28%). The transient spectra (and the square residuals shown here) have been calculated for four different values of the chemical shift ΔE_0: (a) 0 eV, (b) -0.6 eV, (c) -1.2 eV, and (d) -2.5 eV. The χ_r^2 values were obtained by restricting the data to the 1.8–10.1 Å^{-1} range of the LS photoelectron wave vector k.

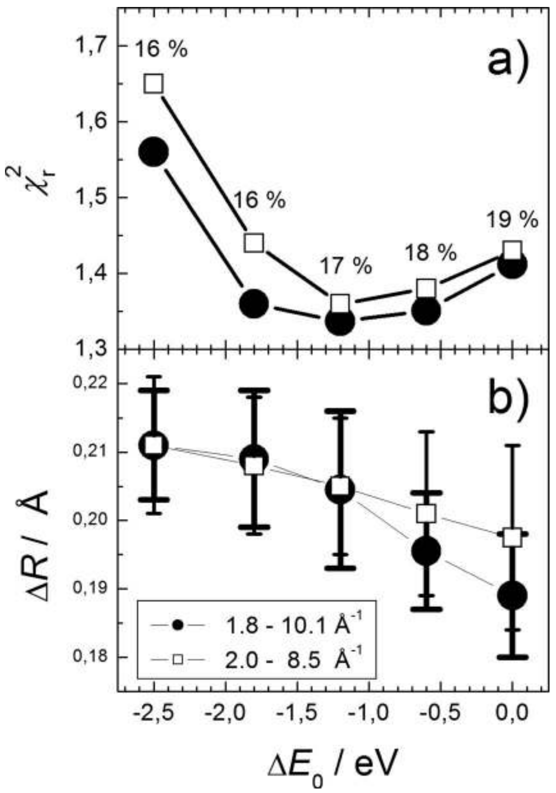

FIG. 6. Least-squares results as a function of ΔE_0 for the calculations shown in Fig. 5 ($\Delta E_0=-1.8$ eV not shown in Fig. 5) for two different k ranges: 1.8–10.1 Å^{-1} (solid circles) and 2–8.5 Å^{-1}. (a) Least-squares values (with their associated fractional population f indicated in percent) and (b) the corresponding Fe–N bond distance. The error bars represent a 95% confidence level. A chemical shift of approximately −1.2 eV can be derived from this analysis, corresponding to a bond elongation of ~0.203 Å for the HS species.

excited state structure or spectrum, due to the additional input about the chemically reasonable excited state structures. It actually also allowed us to determine a third unknown: the value of the chemical shift ΔE_0.

Overall, we observe a roughly linear dependence of the Fe–N bond length with both fractional population f and ΔE_0, ~0.002 Å if f changes by 1%, and ~0.008 Å for varying ΔE_0 by 1 eV. Taking these into account as uncertainties for the HS structure, we determine the Fe–N bond elongation (within a 95% confidence level) to $\Delta R(\mathrm{HS-LS})=0.203(0.008)$ Å with $\Delta E_0=-1.2(0.6)$ eV and $f=17(1)\%$ from the global statistical analysis derived from Figs. 5 and 6. This result is in agreement with the previously reported Fe–N bond elongation value[13] (see Sec. V for more details). With these parameters, we can now compare the best transient model spectrum to the experimental data. For display purposes only we transform it together with the experimental transient measurement into k space (of the LS) and weigh them with k^2. The result is shown in Fig. 8 and the agreement is very satisfactory.

The very accurate determination of $\Delta R(\mathrm{HS-LS})$ allows us to derive the angular change in the N–Fe–N angle in the HS state. Assuming that the length of the rigid interring C═C double bond of the bpy ligand [Fig. 1(b)] remains unchanged in the HS state, the change in N–Fe–N angle in the HS state can be derived from

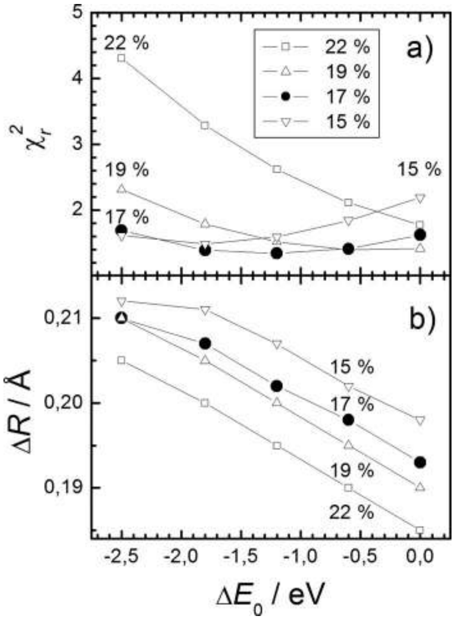

FIG. 7. Least-squares analysis results as a function of ΔE_0 for a constant fractional population of 15% (down triangles), 17% (solid circles), 19% (up triangles), and 22% (open squares). (a) Least-squares values and (b) Fe–N bond elongation. (Error bars have been removed for visibility.)

$$\frac{\sin(\alpha_{\mathrm{LS}}/2)}{\sin(\alpha_{\mathrm{HS}}/2)}=\frac{R_{\mathrm{Fe-N}}^{\mathrm{LS}}+\Delta R(\mathrm{HS-LS})}{R_{\mathrm{Fe-N}}^{\mathrm{LS}}}=1+\frac{\Delta R(\mathrm{HS-LS})}{R_{\mathrm{Fe-N}}^{\mathrm{LS}}}, \tag{13}$$

where α_{LS} and α_{HS} denote LS and HS values of the N–Fe–N angle. For the LS Fe–N distance, we use our optimized value of $R_{\mathrm{Fe-N}}^{\mathrm{LS}}=1.98$ Å and the N–Fe–N angle of 81.6°, which reflects the trigonal distortion imposed by D_3 symmetry onto the octahedral 90° angle.[24] For the HS state we find $\alpha_{\mathrm{HS}}=73°$ using $\Delta R(\mathrm{HS-LS})=0.203(0.008)$ Å. This is different to the 76° HS angle obtained in the density functional theory (DFT) calculations,[24] which would deliver an Fe–N bond elongation of only 0.12 Å that significantly deviates from the

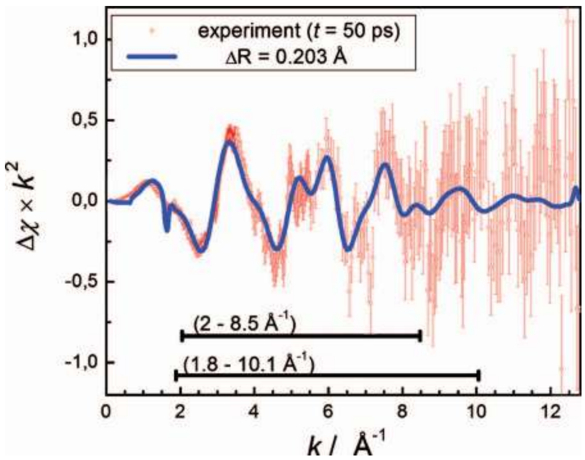

FIG. 8. (Color) Experimental transient absorption spectrum and the least-squares transient simulation (with $\Delta R=0.203$ Å). The different ranges used for the statistical analysis are indicated by the horizontal bars in the graph. The feature near 1.6 Å^{-1} in the simulated transient is an artifact due to the utilized Fourier window for generating the excited state models and was thus excluded from the statistical analysis.

measured values for the HS state of Fe(II)-based SCO complexes.[23] The present analysis assumed a planar bpy structure, but already for the GS and the DFT results for the HS state there is a twist between each pyridine moiety of the bpy ligand, which was measured to 6.4° (LS) in an x-ray crystallographic study[25] and simulated to about 0° (LS) and about 5° (HS) in Ref. 24. The quality of the present transient data is not sufficient to attempt to measure the twist angle within each bpy ligand and is therefore not included in the present analysis.

V. DISCUSSION

The analysis presented here provides a novel and detailed treatment of transient EXAFS measurements in energy space which includes the experimental uncertainty for each data point as the figure of merit [via Eq. (12)]. By moving the entire ligands in discrete steps while respecting the chemical integrity of the sample and analyzing the derived transient spectra together with the experimental transient spectrum after 50 ps, we obtain a convincing result for the HS structure of $[\mathrm{Fe^{II}(bpy)_3}]^{2+}$. We previously reported the analysis of the HS structure of $[\mathrm{Fe^{II}(bpy)_3}]^{2+}$ by analyzing the XANES region,[13] where multiple scattering effects are dominant. This analysis optimized the excited state Fe–N bond distances for the first coordination shell but maintained a constant N–Fe–N angle for all Fe–N distances, which does not rigorously respect the internal structure of the bipyridine ligands. An additional Monte Carlo simulation derived a value for the chemical energy shift of −2.5 eV next to an optimum fractional population of 22%. The results obtained from the current analysis [−1.2(0.6) eV and 17(1)%] correct the previous results, and before discussing the reasons for this discrepancy it is useful to report their implications.

In Fig. 9 we analyze the f-dependence of the bond length change for $\Delta E_0=-1.2$ eV (this work) and $\Delta E_0=-2.5$ eV (from Ref. 13). In both cases the derived bond length changes lie well within the error bars; in addition, the f dependence is so small that $f=17\%$ yields a very similar result as $f=22\%$. The latter value was derived from the time-dependent LS state bleach recovery signal measured by femtosecond transient absorption spectroscopy in the optical domain,[26] which also confirmed the ~0.65 ns population decay time of the $^5T_2$ HS state. In Fig. 10, we compare the HS decay kinetics measured by ultrafast optical transient absorption[26] with the picosecond x-ray absorption experiment.[13] The XAS curve deviates from that measured with femtosecond optical pulses due to convolution of the kinetics with the 70 ps x-ray pulse width. This then leads to the reduced population measured around time zero by the x-ray pulse, as seen in the figure, which merges into the laser measurement at later times. This difference in measured populations amounts to ~20% at $\Delta t=50$ ps, which nicely explains the difference between the fractional population values estimated from both experiments, i.e., 22% (optical) and 17% (x ray).

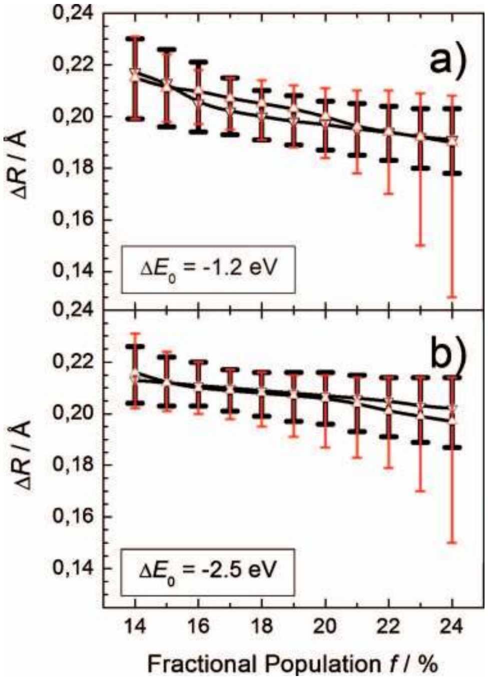

FIG. 9. (Color) Analysis of the Fe–N distance on the fractional population of the HS state population f in the present analysis for using the derived value of (a) $\Delta E_0=-1.2$ eV and using the previously published value of (b) $\Delta E_0=-2.5$ eV in Ref. 13. Both data ranges used for the analysis are displayed (large blue error bars: 1.8–10.1 Å^{-1}, up triangles; small red error bars: 2.0–8.5 Å^{-1}, down triangles). All treatments show very similar results within uncertainty with the smallest uncertainty occurring at $f=17\%$.

Figure 11 summarizes the entire set of results from the present and previous estimates. Figures 11(a) and 11(b) display the results for 95% and 90% confidence level, respectively, with $f=17(1)\%$ and $\Delta E_0=-1.2(0.6)$ eV. Figure 11(c) shows the present analysis result using $\Delta E_0=-2.5(0.5)$ eV and $f=22(1)\%$ from Ref. 13. The mean values differ very little but the uncertainty increases from (a) to (c), but (c) delivers a much worse transient spectrum compared to the other two results. Finally, the mean values and uncertainties are collected from Ref. 13 [Figs. 11(d)–11(f)] which shows the MXAN results after optimizing the chemical shift to $\Delta E_0=-2.5$ eV with an uncertainty of 0.5 eV for a constant $f=22\%$ (d) and optimizing f between 20% and 23% for a

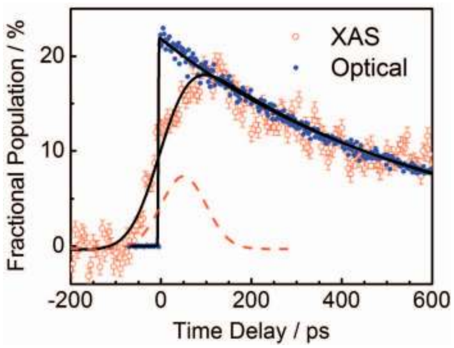

FIG. 10. (Color) Comparison between the transient XAS signal of aqueous $[\mathrm{Fe^{II}(bpy)_3}]^{2+}$ recorded at 7126 eV (open circles with error bars) and the optical femtosecond transient absorption signal (solid circles) together with their fit functions. Both experiments were performed under (nearly) identical laser conditions and have been rescaled and reflect the actual (optical) and convoluted (XAS) fractional population due to the much larger x-ray pulse width. Both populations decay nonradiatively into the GS with a lifetime of 0.6 ns. The dashed Gaussian-shaped line illustrates the x-ray pulse width at the used time delay (50 ps).

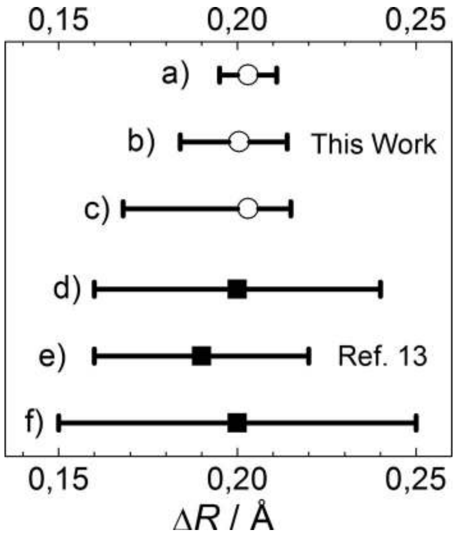

FIG. 11. Fe–N bond elongation determined from different procedures: [(a) and (b)] applying 95% and 90% confidence level from the present analysis, (c) using previously published values $\Delta E_0=-2.5$ eV and $f=22\%$, [(d) and (e)] reproduced from MXAN fits, and (f) from an EXAFS fit of the extracted HS spectrum. [(d)–(f)] Taken from Ref. 13. (For details see text.)

fixed $\Delta E_0=-2.5$ eV (e). Last, (f) shows the result for individual shell fitting of the HS EXAFS spectrum with the ARTEMIS program[27] (using $f=22\%$) and yielding $\Delta E_0=-2.8(0.5)$ eV. All values agree well with the optimum result derived from the present analysis [Fig. 11(a)] but only the results in (a) and (b) deliver acceptable minimized χ_r^2 values around 1.3 (the others lying above or far above 2). Thus the difference between the various analyses does not concern the resulting distances but their output parameters (and strikingly different agreements to the data). The least-squares analysis of Fig. 11(f) ignored the experimental error while the MXAN results [Figs. 11(d) and 11(e)] did include Eq. (10), albeit with a single average error for all data points. In contrast to the current analysis, the fit of XANES in Ref. 13 included the transient data starting at the absorption edge itself and focused on low-*k* values for which multiple scattering is very sensitive to the local environment. This was purposely discarded in the present analysis since the simulated EXAFS focuses on single-scattering events, thus the present analysis commences from ~2 Å^{-1} in wave vector space (Fig. 8) and extends far above the 200 eV range analyzed in the MXAN treatment.

Going back to the different values for the chemical shift we should first clarify the nomenclature. Conventionally, the chemical shift is defined as the energy difference between the bare metal absorption edge and that of the metallic complex[28]

$$\Delta E = E(\text{complex}) - E(\text{metal}), \tag{14}$$

TABLE I. Structural parameters (Fe–N bond distance R_{FeN} and N–Fe–N bond angle α) of the LS state of $[\text{Fe}^{\text{II}}(\text{bpy})_3]^{2+}$ in H_2O and their changes in going from the LS to the HS state along with the chemical shift (ΔE) and the photoexcitation yield (f) derived from the present EXAFS analysis (uncertainties are given in brackets). The present parameters correct those previously published.

	LS: $R_{\text{Fe–N}}/\text{Å}$ HS−LS: $\Delta R_{\text{Fe–N}}/\text{Å}$	LS: $\alpha/°$ HS−LS: $\Delta\alpha/°$	$\Delta E/\text{eV}$	$f(\text{HS})/\%$
LS	1.98(0.01)	81.6(0.3)		
HS−LS	0.203(0.008)	−8.8(0.3)	−1.2 (0.6)	17 (1)

which yields rather large values on the order of 5–10 eV.[29] A more common definition of the chemical shift deals with the observed differences in complexes when the metal atom has a different valency

$$\Delta E = E(\text{valency} + 1) - E(\text{valency}) \tag{15}$$

and typical values are around 1–2 eV.[30] We observed such a shift in our picosecond XAS study of the light induced electron transfer process in aqueous $[\text{Ru}^{\text{II}}(\text{bpy})_3]^{2+}$.[12] In the present case, the LS and HS states correspond to the same oxidation state of the Fe atom, but the electronic configuration changes from $3d(t_{2g}^6)$ to $3d(t_{2g}^4e_g^2)$ (here we use the nomenclature of orbitals in the O_h ligand field of the system). This represents a significant electronic structure change (after all, the HS electronic structure causes a dramatic increase in the Fe–N distance by ~10%). It is a well established fact that the ionization potential of molecules is configuration dependent, as evidenced in ultrafast photoelectron spectroscopy studies of gas phase molecules.[31] However, for metal-based complexes it is not evident to predict neither the direction of the shift nor its magnitude. Ligand field effects were investigated in detail on several Cu(II) compounds delivering values on the order of up to 1–1.5 eV and have been related to the change in crystal field splitting between both compounds.[32] These energy shifts thus correspond to the present definition of ΔE_0 [Eq. (7)] and the change in crystal field splitting (10Dq) in the Fe 3*d* levels between LS and HS $[\text{Fe}^{\text{II}}(\text{bpy})_3]^{2+}$ is around 1.6 eV,[33] which therefore allows the result of −1.2 (0.6) eV reported here. Note that 10Dq changes depend also on the presence of the core hole; therefore the optically derived changes in 10Dq are less than 1 eV. Thus, in addition to retrieving an accurate value of the fractional population of excited species, the present statistical analysis also brackets the magnitude of the chemical shift in a range of physically meaningful values. By analyzing the least-squares residuals of the transient simulations with the transient data we obtain a precise value for the nearest neighbor Fe–N distance of 0.203 (0.008) Å within 95% confidence level. The retrieved structural and nonstructural fit parameters of the HS state are given in Table I, along with the structural parameters of the LS GS.

VI. CONCLUSIONS

This work presents a detailed statistical analysis of the measured transient EXAFS in energy space to derive with high precision the bond length *changes*. We applied it to the case of the structural changes resulting from the photoinduced spin-crossover process in $[\text{Fe}^{\text{II}}(\text{bpy})_3]^{2+}$. In such an analysis the uncertainties of the nonstructural parameters cancel out to a high degree and the derived distance changes maintain an exceptionally low uncertainty despite the rather average quality of the transient data. An important point of this treatment lies in the fact that the structural integrity of the ligand system is strictly conserved by calculating a series of EXAFS spectra with stepwise increasing distances between the Fe central atom and the bpy ligands. The treatment also retrieves physically reasonable values of the chemical energy shift in the absorption edge between both states. It also shows the sensitive interplay between structural determination and fractional population, which was already stressed as being crucial in the analysis of time-resolved XAS experiments.[4] This treatment allows extracting an unknown (excited state) structure *together* with an unknown fractional population, starting only from TA data and the GS EXAFS. This is usually impossible in an unambiguous way since one seeks to solve Eq. (2) with two unknowns. But in the present analysis we were able to apply prior knowledge about the *possible* excited state structures, and this restriction (=additional knowledge about the excited state system) led to one single solution for both unknown parameters, of which one (the population) was in excellent agreement with independent laser measurements. This treatment should have implications on the study of photoexcited samples, for which the excited state population may not be precisely retrievable by laser-only measurements. In the present system, only one coordinate (the Fe-ligand distance) is changing. However, the increased structural accuracy reached by the present procedure allows us now to determine more than one type of bond structure change. This was recently achieved for the triplet excited state of a more complex system: $[Pt_2(P_2O_5H_2)_4]^{4-}$ in solution, while retrieving a reasonable value of f.[34] Finally, the present procedure should also aid in our goal to analyze unknown transient structures on the femtosecond time scale.

ACKNOWLEDGMENTS

This work was funded by the Swiss National Science Foundation via Contract Nos. 620–066145, 200021–107956, PP002–110464, 200020–116023, 200021–105239, and 200020-116533.

[1] C. Bressler and M. Chergui, Chem. Rev. (Washington, D.C.) **104**, 1781 (2004).

[2] L. X. Chen, Angew. Chem., Int. Ed. **43**, 2886 (2004).

[3] A. H. Zewail, Annu. Rev. Phys. Chem. **57**, 65 (2006); M. Bargheer, N. Zhavoronkov, M. Woerner, and T. Elsaesser, ChemPhysChem **7**, 783 (2006); M. Chergui and A. H. Zewail, *ibid.* **10**, 28 (2009).

[4] C. Bressler, R. Abela, and M. Chergui, Z. Kristallogr. **223**, 307 (2008).

[5] M. Khalil, M. A. Marcus, A. L. Smeigh, J. K. McCusker, H. H. W. Chong, and R. W. Schoenlein, J. Phys. Chem. A **110**, 38 (2006).

[6] R. W. Schoenlein, S. Chattopadhyay, H. H. W. Chong, T. E. Glover, P. A. Heimann, W. P. Leemans, C. V. Shank, A. Zholents, and M. Zolotorev, Appl. Phys. B: Lasers Opt. **71**, 1 (2000); S. Khan, K. Holldack, T. Kachel, R. Mitzner, and T. Quast, Phys. Rev. Lett. **97**, 074801 (2006); P. Beaud, S. L. Johnson, A. Streun, R. Abela, D. Abramsohn, D. Grolimund, F. Krasniqi, T. Schmidt, V. Schlott, and G. Ingold, *ibid.* **99**, 174801 (2007).

[7] C. Bressler, C. J. Milne, V. T. Pham, A. Al Nahhas, R. M. van der Veen, W. Gawelda, S. Johnson, P. Beaud, D. Grolimund, M. Kaiser, C. N. Borca, G. Ingold, R. Abela, and M. Chergui, Science **323**, 489 (2009).

[8] A. H. Zewail, Angew. Chem., Int. Ed. **39**, 2587 (2000).

[9] M. Saes, C. Bressler, F. van Mourik, W. Gawelda, M. Kaiser, M. Chergui, C. Bressler, D. Grolimund, R. Abela, T. E. Glover, P. A. Heimann, R. W. Schoenlein, S. L. Johnson, A. M. Lindenberg, and R. W. Falcone, Rev. Sci. Instrum. **75**, 24 (2004).

[10] M. Saes, W. Gawelda, M. Kaiser, A. Tarnovsky, C. Bressler, M. Chergui, S. L. Johnson, D. Grolimund, and R. Abela, Synchrotron Radiat. News **16**, 12 (2003).

[11] M. Saes, C. Bressler, R. Abela, D. Grolimund, S. L. Johnson, P. A. Heimann, and M. Chergui, Phys. Rev. Lett. **90**, 047403 (2003).

[12] W. Gawelda, M. Johnson, F. M. F. de Groot, R. Abela, C. Bressler, and M. Chergui, J. Am. Chem. Soc. **128**, 5001 (2006).

[13] W. Gawelda, V. T. Pham, M. Benfatto, Y. Zaushytsin, M. Kaiser, D. Grolimund, S. Johnson, R. Abela, C. Bressler, and M. Chergui, Phys. Rev. Lett. **98**, 057401 (2007).

[14] V. T. Pham, W. Gawelda, Y. Zaushytsin, M. Kaiser, D. Grolimund, S. Johnson, R. Abela, C. Bressler, and M. Chergui, J. Am. Chem. Soc. **129**, 1530 (2007).

[15] R. F. Pettifer, O. Mathon, S. Pascarelli, M. D. Cooke, and M. R. J. Gibbs, Nature (London) **435**, 78 (2005).

[16] W. Gawelda, "Time-resolved x-ray absorption spectroscopy of transition metal complexes," Ph.D. Thesis, Ecole Polytechnique Fédérale de Lausanne, Lausanne, Switzerland, 2006.

[17] C. Consani, M. Prémont-Schwarz, A. El Nahhas, C. Bressler, F. van Mourik, A. Cannizzo, and M. Chergui, "Femtosecond UV probe spectroscopy of light-induced spin cross-over in aqueous $[Fe^{II}(bpy)_3]^{2+}$," J. Am. Chem. Soc. (submitted).

[18] A. L. Ankudinov, B. Ravel, J. J. Rehr, and S. D. Conradson, Phys. Rev. B **58**, 7565 (1998).

[19] C. Code, http://accelrys.com/products/cerius2/.

[20] S. Dick, Z. Kristallogr.-New Cryst. Struct. **213**, 356 (1998).

[21] W. Gawelda, V. T. Pham, A. El Nahhas, M. Kaiser, Y. Zaushytsin, S. Johnson, D. Grolimund, R. Abela, A. Hauser, C. Bressler, and M. Chergui, AIP Conf. Proc. **882**, 31 (2007).

[22] P. Guionneau, J. F. Letard, D. S. Yufit, D. Chasseau, G. Bravic, A. E. Goeta, J. A. K. Howard, and O. Kahn, J. Mater. Chem. **9**, 985 (1999).

[23] P. Guionneau, M. Marchivie, G. Bravic, J. F. Letard, and D. Chasseau, Top. Curr. Chem. **234**, 97 (2004).

[24] L. M. Lawson Daku, A. Vargas, A. Hauser, A. Fouqueau, and M. E. Casida, ChemPhysChem **6**, 1393 (2005).

[25] K. B. Wiberg, P. R. Rablen, D. J. Rush, and T. A. Keith, J. Am. Chem. Soc. **117**, 4261 (1995).

[26] W. Gawelda, A. Cannizzo, V. T. Pham, F. van Mourik, C. Bressler, and M. Chergui, J. Am. Chem. Soc. **129**, 8199 (2007).

[27] B. Ravel and M. Newville, J. Synchrotron Radiat. **12**, 537 (2005).

[28] B. D. Shrivastava, B. D. Shrivastava, S. K. Joshi, K. B. Pandey, and A. Mishra, J. Synchrotron Radiat. **8**, 713 (2001).

[29] A. N. Mansour and C. A. Melendres, J. Phys. Chem. A **102**, 65 (1998).

[30] F. M. F. de Groot, Z. W. Hu, M. F. Lopez, G. Kaindl, F. Guillot, and M. Tronc, J. Chem. Phys. **101**, 6570 (1994).

[31] A. Stolow, Annu. Rev. Phys. Chem. **54**, 89 (2003).

[32] K. Shimizu, H. Maeshima, H. Yoshida, A. Satsuma, and T. Hattori, Phys. Chem. Chem. Phys. **3**, 862 (2001).

[33] F. M. F. de Groot, Coord. Chem. Rev. **249**, 31 (2005).

[34] R. M. van der Veen, C. J. Milne, J. Best, J. A. Weinstein, A. El Nahhas, V. T. Pham, F. Lima, C. Bressler, and M. Chergui, Angew. Chem., Int. Ed. **40**, 2711 (2009).